

Magnetotransport properties of two-dimensional fermionic systems with k -cubic Rashba spin-orbit interaction

Alestin Mawrie, Tutul Biswas and Tarun Kanti Ghosh

Department of Physics, Indian Institute of Technology-Kanpur, Kanpur-208 016, India

(Dated: October 6, 2018)

The spin-orbit interaction in heavy hole gas formed at p -doped semiconductor heterojunctions and electron gas at SrTiO₃ surfaces is cubic in momentum. Here we report magnetotransport properties of k -cubic Rashba spin-orbit coupled two-dimensional fermionic systems. We study longitudinal and Hall component of the resistivity tensor analytically as well as numerically. The longitudinal resistivity shows beating pattern due to different Shubnikov-de Haas (SdH) oscillation frequencies f_{\pm} for spin-up and spin-down fermions. We propose empirical forms of f_{\pm} as exact expressions are not available, which are being used to find location of the beating nodes. The beating nodes and the number of oscillations between any two successive nodes obtained from exact numerical results are in excellent agreement with those calculated from the proposed empirical formula. In the Hall resistivity, an additional Hall plateau appears in between two conventional ones as spin-orbit coupling constant increases. The width of this additional plateau increases with spin-orbit coupling constant.

PACS numbers: 73.61.Ey, 73.21.Fg, 71.43.-f, 71.70.Ej.

I. INTRODUCTION

The spin degeneracy of a charge carrier in condensed matter systems is a result of spatial inversion symmetry and time-reversal symmetry together. The spin degeneracy is lifted if one of the symmetries is absent. The electric field normal to the interface of III-V semiconductor quantum well (such as GaAs/AlGaAs heterostructure) breaks the spatial inversion symmetry. The symmetry breaking electric field gives rise to spin-orbit interaction (SOI) which breaks the spin degeneracy even in absence of an external magnetic field. The dominant SOI in two-dimensional electron gas (2DEG) formed at the interface of GaAs/AlGaAs heterostructure is linear in momentum and it is known as Rashba SOI.^{1,2} Moreover, the Rashba SOI strength can be controlled with the help of an external bias.³⁻⁵ The SOI is essential to control and manipulate spin degree of freedom of a charge carrier. After the proposal of spin field effect transistor by Datta and Das,⁶ a large number of theoretical and experimental studies have been performed in the emerging field of spintronics⁷⁻⁹ for the possibility of detecting pure spin current. The Rashba SOI need not be always linear in momentum. There are couple of systems where the Rashba SOI is cubic in momentum. Two such systems are two-dimensional hole gas (2DHG)¹⁰⁻¹³ formed at p -doped GaAs/AlGaAs heterojunction and 2DEG at SrTiO₃ surfaces.^{14,15} Very recently, it is reported in Ref.¹⁶ that k^3 SOI is dominating in a two-dimensional hole gas formed in a strained Ge/SiGe quantum well.

In general, 4×4 Luttinger Hamiltonian^{17,18} describes 2DHG formed at p -doped semiconductor quantum well. At very low temperature and low density only the lowest heavy hole (HH) sub-bands are occupied. The projection of 4×4 Luttinger Hamiltonian onto the HH states $|3/2, \pm 3/2\rangle$ leads to an effective k -cubic^{11,12}

Rashba SOI. This SOI opens up a gap $\Delta_{\text{so}} = 2\alpha k_F^3$ (where α is the Rashba spin-orbit coupling constant and k_F is the Fermi wave vector) between two spin-split heavy hole sub-bands. This spin splitting has been observed experimentally¹⁹ for holes in C-doped p -type GaAs/AlGaAs quantum well and the value of Δ_{so} is also extracted by analyzing the beating pattern in the SdH oscillations as well as by using weak anti-localization method. In recent past a number of investigations have been performed to explore various properties of 2DHG like effective mass,²⁰⁻²² effective g factor,²³ spin polarization,²⁴ spin rotation²⁵ etc. Most importantly, spin Hall effect^{12,26-31} in 2DHG has been studied experimentally as well as theoretically.

On the other hand, three 3d orbitals (t_{2g} : d_{xy}, d_{xz}, d_{yz}) of Ti ion form the conduction band^{32,33} of SrTiO₃ crystal. The 3d orbitals at the surface are confined in the z -direction which is normal to the interface. As a result it yields a 2DEG. The lowest energy states of the bulk SrTiO₃ are fourfold degenerate bands, corresponds to the states $|3/2, \pm 3/2\rangle$ and $|3/2, \pm 1/2\rangle$. Various studies^{34,35} suggest that the confinement along the z direction lifts the Γ -point degeneracy between the d_{xy} band and d_{xz}, d_{yz} bands. Within the effective tight-binding Hamiltonian for t_{2g} bands of SrTiO₃ surfaces, the Rashba SOI is cubic in momentum. There is an experimental evidence¹⁴ of k -cubic Rashba SOI on SrTiO₃ surfaces.

In this work we study magnetotransport coefficients of fermions with k -cubic Rashba spin-orbit interaction. The longitudinal conductivity which arises entirely due to the collision or hopping process exhibits beating pattern. We provide two empirical frequencies f_{\pm} of quantum oscillations of spin-up and spin-down fermions, which are responsible for the beating pattern. At higher values of magnetic field the beating pattern is replaced by resistivity peak. As α increases, the peak in the resistivity splits into two asymmetric ones. On the other hand, Hall con-

ductivity shows the conventional plateau structure. With the increase of α an additional plateau arises between two conventional ones. The width of this additional plateau increases with α .

This paper is organized as follows. In section II, we present the basic informations about the k -cubic spin-orbit coupled fermions. In section III, analytical calculations for the different transport coefficients are given. Numerical results and discussion are presented in section IV. We summarize our results in section V.

II. BASIC INFORMATIONS

The Hamiltonian for a fermion with k -cubic spin-orbit interaction in presence of a magnetic field $\mathbf{B} = B\hat{z}$ is given by^{36,37}

$$H = \frac{\mathbf{\Pi}^2}{2m^*} + \frac{i\alpha}{2\hbar^3}(\mathbf{\Pi}_-^3\sigma_+ - \mathbf{\Pi}_+^3\sigma_-) - \frac{3}{2}g^*\mu_B\boldsymbol{\sigma} \cdot \mathbf{B}, \quad (1)$$

where $\mathbf{\Pi} = \mathbf{p} - e\mathbf{A}$ with \mathbf{A} is the vector potential, m^* is the effective mass of the fermion and α is Rashba spin-orbit coupling constant. Also, $p_{\pm} = p_x \pm ip_y$, $\sigma_{\pm} = \sigma_x \pm i\sigma_y$ with σ_i 's are the Pauli matrices, g^* is the effective Lande- g factor and μ_B is the Bohr magneton.

Using the Landau gauge $\mathbf{A} = (0, xB, 0)$, the Hamiltonian given by Eq. (1) commutes with p_y i.e. k_y is a good quantum number in this case. The energy eigen value for $n \geq 3$ is given by

$$E_n^\lambda = \hbar\omega_c \left[n - 1 + \lambda \sqrt{\tilde{E}_{n\alpha}^2 + \tilde{E}_0^2} \right], \quad (2)$$

where $\lambda = \pm$, $\tilde{E}_0 = 3/2 - \chi$ with $\chi = 3g^*m^*/(4m_0)$, $\tilde{E}_{n\alpha} = \tilde{\alpha}\sqrt{8n(n-1)(n-2)}$. Here $\tilde{\alpha}$ is defined as $\tilde{\alpha} = l_\alpha/l_c$ with $l_\alpha = m^*\alpha/\hbar^2$ and $l_c = \sqrt{\hbar/(eB)}$ is the magnetic length. The corresponding eigenstates for positive and negative branches are given by

$$\psi_{n,k_y}^+(x, y) = \frac{e^{ik_y y}}{\sqrt{L_y A_n}} \begin{pmatrix} \phi_n(X) \\ D_n \phi_{n-3}(X) \end{pmatrix} \quad (3)$$

and

$$\psi_{n,k_y}^-(x, y) = \frac{e^{ik_y y}}{\sqrt{L_y A_n}} \begin{pmatrix} -D_n \phi_n(X) \\ \phi_{n-3}(X) \end{pmatrix}, \quad (4)$$

where L_y is the system length along y -direction, $X = x - x_c$ with $x_c = k_y l_c^2$ and $A_n = 1 + D_n^2$ with $D_n = \tilde{E}_{n\alpha} / (\tilde{E}_0 + \sqrt{\tilde{E}_0^2 + \tilde{E}_{n\alpha}^2})$. Here $\phi_n(x)$ is the oscillator wave function of order n .

For $n < 3$ there is only one branch (+ branch). In this case the eigenvalues and eigen functions are given by

$$E_n = \hbar\omega_c (n + 1/2 - \chi) \quad (5)$$

and

$$\psi_{n,k_y}(x, y) = \frac{e^{ik_y y}}{\sqrt{L_y}} \phi_n(X) \begin{pmatrix} 1 \\ 0 \end{pmatrix}. \quad (6)$$

The derivation of the energy spectrum and the corresponding eigenfunctions are given in Appendix A.

III. DERIVATION OF MAGNETOTRANSPORT COEFFICIENTS

In this section we calculate both the longitudinal and transverse components of conductivity tensor using Kubo formula.³⁸ The longitudinal conductivity contains diffusive and collisional contribution. In presence of a perpendicular magnetic field the diagonal matrix elements of velocity operator become zero which in turn causes the vanishing of diffusive conductivity. So the longitudinal conductivity is solely due to the collisional contribution.

Collisional conductivity: At low temperature, one can safely assume that fermions are elastically scattered by charged impurities distributed uniformly over the system. The expression for collisional conductivity is given by³⁹⁻⁴³

$$\sigma_{xx}^{\text{coll}} = \frac{\beta e^2}{\Omega} \sum_{\xi, \xi'} f(E_\xi) \{1 - f(E_{\xi'})\} W_{\xi\xi'} (x^\xi - x^{\xi'})^2 \quad (7)$$

Here $|\xi\rangle = |n, k_y, \lambda\rangle$ defines a set of all quantum numbers, Ω is the surface area of the two-dimensional system, $f(E_\xi) = 1/(\exp((E_\xi - \mu)\beta) + 1)$ is the Fermi distribution function with $\beta = 1/(k_B T)$ and $x^\xi = \langle \xi | x | \xi \rangle = k_y l_c^2$ is the expectation value of the x component of the position operator. Finally, the transition probability between two states $|\xi\rangle$ and $|\xi'\rangle$ is given by

$$W_{\xi\xi'} = \frac{2\pi n_{\text{im}}}{\hbar\Omega} \sum_{\mathbf{q}} |U(\mathbf{q})|^2 |F_{\xi, \xi'}|^2 \delta(E_\xi - E_{\xi'}), \quad (8)$$

where n_{im} is the impurity density and $U(\mathbf{q}) = e^2/(2\epsilon_0\epsilon(q^2 + k_s^2)^{1/2})$ is the Fourier transform of the screened Yukawa-type impurity potential $U(r) = e^2 e^{-k_s r}/(4\pi\epsilon_0\epsilon r)$ with ϵ , ϵ_0 and k_s as the dielectric constant of the medium, the vacuum permittivity and the screened wave vector, respectively. The term $F_{\xi, \xi'} = \langle \xi | e^{i\mathbf{q}\cdot\mathbf{r}} | \xi' \rangle$ is called form factor whose complete expression is given in Appendix B. Since the term $F_{\xi, \xi'}$ is proportional to $\delta_{k'_y, k_y + q_y}$, the summation over k'_y in Eq. (7) can be easily evaluated with the replacement of k'_y by $k_y + q_y$ and we have $(x^\xi - x^{\xi'}) = q_y^2 l_c^4 = q^2 l_c^4 \sin^2 \phi$. The delta function in Eq. (8), $\delta(E_\xi - E_{\xi'}) = \delta(E_n^\lambda - E_{n'}^{\lambda'})$, ensures the possibilities of only intra-branch and intra-level scattering i.e. $n' = n$ and $\lambda' = \lambda$. Again $\delta(E_n^\lambda - E_{n'}^{\lambda'})$ can be written in its usual Lorentzian representation i.e. $\delta(E_n^\lambda - E_{n'}^{\lambda'}) = (1/\pi)\Gamma/[(E_n^\lambda - E_{n'}^{\lambda'})^2 + \Gamma^2]$ with Γ is the impurity induced Landau level broadening. We also have $\sum_{k_y} \rightarrow \Omega/(2\pi l_c^2)$ and $\sum_{\mathbf{q}} \rightarrow (\Omega/(2\pi)^2) \int q dq d\phi$. So by inserting Eq. (8) into Eq. (7) and after doing all the summations one can obtain the following expression of the collisional conductivity:

$$\begin{aligned} \sigma_{xx}^{\text{coll}} &= \frac{e^2}{h} \frac{\beta n_i l_c^2 U_0^2}{2\pi\Gamma} \sum_{n,\lambda} f(E_n^\lambda) \{1 - f(E_n^\lambda)\} \\ &\times \int dq q^3 |F_{nn}^\lambda(q)|^2. \end{aligned} \quad (9)$$

In deriving Eq. (9) we have used the following approximation $|U(q)| \simeq U_0 = e^2/(2\epsilon_0\epsilon k_s)$ since $q \ll k_s$. Now using the fact $n_{\text{im}}U_0^2 \sim (\Gamma l_c)^2/(4\pi)$, we finally have

$$\sigma_{xx}^{\text{coll}} = \frac{e^2}{h} \frac{\beta\Gamma}{4\pi^2} \sum_{n,\lambda} f(E_n^\lambda) \{1 - f(E_n^\lambda)\} I_n^\lambda, \quad (10)$$

where $I_n^\lambda = \int_0^\infty u du |F_{nn}^\lambda|^2$ with $u = q^2 l_c^2/2$. It is straightforward to evaluate the expression of I_n^λ as given by $I_{n<3} = 2n+1$ and $I_{n>3} = \{(2n-2-\lambda 3)(D_n^4+1)+\lambda 6\}/A_n^2$.

Hall conductivity: The expression for the Hall conductivity σ_{yx} is given by⁴¹⁻⁴³

$$\sigma_{yx} = \frac{i\hbar e^2}{\Omega} \sum_{\xi \neq \xi'} \langle \xi | v_y | \xi' \rangle \langle \xi' | v_x | \xi \rangle \frac{f(E_\xi) - f(E_{\xi'})}{(E_\xi - E_{\xi'})^2} \quad (11)$$

The matrix elements of the components of the velocity operator are given in Appendix C. By virtue of the Kronecker delta symbols in Eqs. (C3-C10), it is confirmed that the transitions are allowed only between the adjacent Landau levels $n' = n \pm 1$. We mention here that inter-branch transitions also possible along with the intra-branch scattering. So the summation in Eq. (11) can be split into four terms as $\sigma_{yx} = \sigma_{yx}^{++} + \sigma_{yx}^{--} + \sigma_{yx}^{+-} + \sigma_{yx}^{-+}$, where the first two terms correspond to the intra-branch transition and the last two terms correspond to the inter-branch transition. Setting $\tilde{E}_n^\lambda = E_n^\lambda/(\hbar\omega_c)$, the total Hall conductivity is given by

$$\begin{aligned} \sigma_{yx} &= \frac{e^2}{h} \left[\sum_{n=0}^1 (n+1) \{f(E_n) - f(E_{n+1})\} \right. \\ &+ \sum_{\lambda} \frac{f(E_2) - f(E_3^\lambda)}{(\tilde{E}_2 - \tilde{E}_{3\lambda})^2} C_{23}^\lambda \\ &+ \sum_{\lambda, n=3}^{\infty} \left\{ C_n^{\lambda^2} \frac{f(E_n^\lambda) - f(E_{n+1}^\lambda)}{(\tilde{E}_n^\lambda - \tilde{E}_{n+1}^\lambda)^2} \right. \\ &\left. + C_n^{\lambda^2} \frac{f(E_n^{-\lambda}) - f(E_{n+1}^{-\lambda})}{(\tilde{E}_n^{-\lambda} - \tilde{E}_{n+1}^{-\lambda})^2} \right\} \Big], \end{aligned} \quad (12)$$

where $C_{23}^+ = (\sqrt{3}/2 + 6\sqrt{2}\tilde{\alpha}D_3)^2$, $C_{23}^- = (-D_3\sqrt{3}/2 + 6\sqrt{2}\tilde{\alpha})^2$, $C_n^+ = B_n$, $C_n^- = K_n$, $C_n'^+ = B'_n$ and $C_n'^- = K'_n$ are given in Appendix B.

IV. NUMERICAL RESULTS AND DISCUSSION

In this section we shall present numerical results of Eqs. (10) and (12). Typical system parameters of p-type

GaAs/AlGaAs heterostructure and SrTiO₃ materials are summarized here. For 2DHG, $n_f = 2.03 \times 10^{15} \text{ m}^{-2}$ is the charge carrier density, $m^* = 0.41m_0$ with m_0 as the free electron mass and $g^* = 6.5$. For SrTiO₃ materials^{14,44}, $n_f = 2.4 - 4.7 \times 10^{16} \text{ m}^{-2}$, $m^* = 1.5m_0$ and $g^* = 2$. The Landau level broadening is assumed to be $\Gamma = 0.01 \text{ meV}$. Note that $\Gamma \ll \Delta_{\text{so}} \ll \hbar\omega_c$ ⁴⁵ so that Γ does not blurred the discrete spectrum completely. For various plots, we adopt the parameters of GaAs/AlGaAs heterostructure.

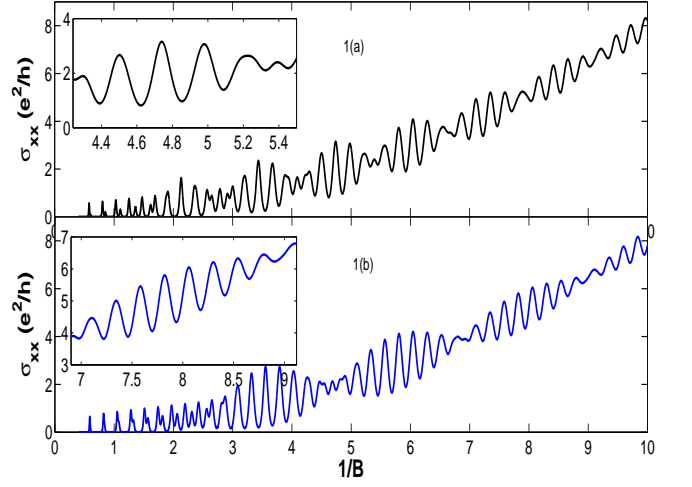


FIG. 1: (color online) Plot of σ_{xx} as a function of $1/B$. The upper panel (1(a)) is for $\alpha = 0.080 \text{ eVnm}^3$ and the lower panel (1(b)) is for $\alpha = 0.048 \text{ eVnm}^3$. The oscillations between 3^{rd} and 4^{th} nodes are shown in insets.

Earlier the spin-splitting and hence the value of α was determined from the difference between the two spin-split heavy hole subband densities.^{13,19} The population densities in the two spin-split sub-bands are measured by analyzing the SdH oscillation frequencies⁴⁶. In the present study we give an alternative treatment for determining α by simply counting the number of oscillations between two beating nodes.

In Fig. 1 we show the variation of σ_{xx} with the inverse magnetic field for two different values of α : $\alpha = 0.08 \text{ eVnm}^3$ and $\alpha = 0.048 \text{ eVnm}^3$. Figure 1 clearly shows regular beating pattern formation in σ_{xx} . Unlike the case of 2DEG with Rashba SOI,⁴⁷ it is not possible to get an analytical expression of the density of states of Landau levels for two-dimensional fermions with k -cubic Rashba SOI. It hinders to have closed-form analytical expression of σ_{xx} . At the same time, exact positions of the nodes would help us to determine the value of α . To obtain the exact locations of the nodes as shown in Fig. 1, we model σ_{xx} as

$$\sigma_{xx} \propto \cos(2\pi f_a/B) \cos(2\pi f_d/B), \quad (13)$$

where $f_a = (f_+ + f_-)/2$ and $f_d = (f_+ - f_-)/2$ with f_{\pm} are the SdH oscillation frequencies for spin-up and spin-down fermions.

Careful observations reveal that the SdH oscillation frequencies for spin-up and spin-down electron in spin-orbit coupled 2DEG are directly related to the spin-split Landau levels. The approximate SdH oscillation frequencies can be obtained by setting $n = n_F$, where n_F is the Landau level quantum number corresponds to the Fermi energy E_F , in the spin-split Landau levels. Using the same analogy for k -cubic spin-orbit coupled systems, we propose f_{\pm} will have the following forms

$$f_{\pm} = \frac{m^*}{\hbar e} \left(E_F^0 \mp \sqrt{\frac{8\alpha^2 (m^* E_F^0)^3}{\hbar^6} + E_0^2} \right), \quad (14)$$

where $E_F^0 = (\hbar k_F^0)^2 / (2m^*)$ with $k_F^0 = \sqrt{2\pi n_f}$.

Now the beating nodes are simply given by $2f_d/B_j = (j + 1/2)$ with $j = 1, 2, \dots$. Using Eq. (14) we obtain the locations of the nodes at

$$\frac{1}{B_j} = \frac{e\hbar}{8\pi\alpha n_f m^*} \sqrt{\frac{(2j+1)^2 - 4(3-2\chi)^2}{2\pi n_f}}. \quad (15)$$

The number of oscillations between any two successive nodes is given by

$$N_{\text{osc}} = f_a \Delta \left(\frac{1}{B} \right) = \left(\frac{m^* E_F^0}{\hbar e} \right) \left(\frac{1}{B_j} - \frac{1}{B_{j+1}} \right). \quad (16)$$

It is straightforward to find the expression for α by solving Eq. (15) and (16) as

$$\alpha = A \left(\sqrt{(2j+3)^2 - C^2} - \sqrt{(2j+1)^2 - C^2} \right), \quad (17)$$

where $A = \hbar^3 / (N_{\text{osc}} \sqrt{128m^* E_F^0})$ and $C = 2(3 - 2\chi)$.

Let us now check whether the results for the locations of nodes and for the number of oscillations N_{osc} , given by Eqs. (15) and (16), obtained based on empirical expressions for f_{\pm} match with the exact numerical results given in Fig. 1. The positions of nodes calculated from both approach are summarized in table I. Moreover, the inset of Fig. 1 shows the number of oscillations between two successive beating nodes. As seen from the inset there are 5 and 9 oscillations between 3rd and 4th nodes in Fig. 1(a) and Fig.1(b), respectively, which are same as calculated from Eq. (16). Again, the calculated strength of Rashba SOI (α) taking $j = 3$ in Eq.(17) are $\alpha = 0.0799$ eVnm³ and $\alpha = 0.0473$ eVnm³, respectively. Thus the numerical and approximate results are in excellent agreement.

To see the high magnetic field behavior of the longitudinal resistivity, it is convenient to plot ρ_{yy} vs magnetic field B . In Fig. 2 we plot longitudinal resistivity ρ_{yy} versus magnetic field B for different values of α . The height of the peaks in the SdH oscillations reduce with the increase of α . It shows that at low B field ($B < 0.5$ T) the regular beating pattern appears in the SdH oscillations. At high magnetic field, the SOI effect is reduced and the resistivity peaks split into two, instead of showing the regular beating pattern.

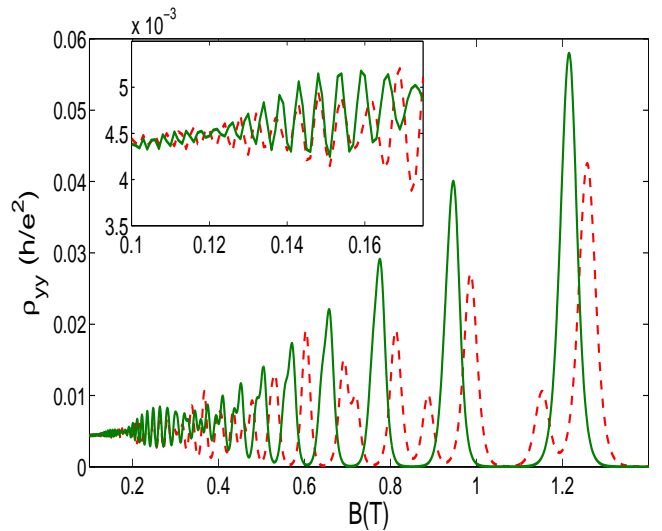


FIG. 2: (color online) Plot of the collisional resistivity ρ_{yy} as a function of magnetic field B for $\alpha = 0.04$ eVnm³ (solid green) and $\alpha = 0.10$ eVnm³ (dashed red). Inset shows the beating patterns in the low magnetic field range.

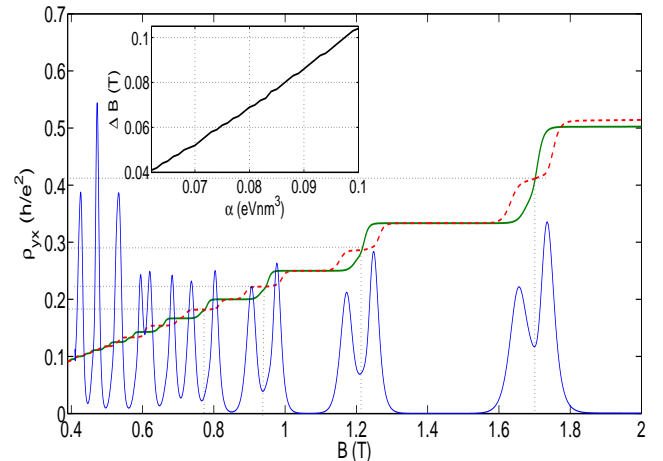


FIG. 3: (color online) Plot of the Hall resistivity ρ_{yx} vs B for $\alpha = 0.04$ eVnm³ (solid green) and $\alpha = 0.10$ eVnm³ (dashed red). The curve shown in blue thin line is the plot of $d\rho_{yx}/dB$ for $\alpha = 0.10$ eVnm³. In the inset the width of the additional plateau is plotted vs α around $B=1.2$ T.

Figure 3 shows the variation of the Hall resistivity ρ_{yx} versus magnetic field B for two different values of α . One can see that the integer quantum Hall plateaus occur at $h/(e^2 N)$, where N is integer. It is interesting to note that as α increases there is an additional plateau at $h/(e^2(N + 1/2))$ appearing between any two conventional plateaus. On the other hand, one can find from the inset of Fig. 3 that the width of the additional plateau increases with increasing α . In Fig. 3 we also plot $d\rho_{yx}/dB$

TABLE I: Beating nodes calculated from Eq. (15) and obtained from Fig. 1 are tabulated here.

α	0.048 eVnm ³		0.080 eVnm ³	
j	Fig. 1(b)	Eq. (15)	Fig. 1(a)	Eq. (15)
1	2.730	2.375	1.710	1.425
2	4.960	4.861	3.070	2.916
3	7.075	7.114	4.260	4.268
4	9.295	9.305	5.550	5.583
5	-	-	6.675	6.882
6	-	-	8.010	8.172
7	-	-	9.340	9.458

versus B as shown by thin line. The sudden jump in the conventional Hall resistivity is characterized by the peaks in $d\rho_{yx}/dB$. These peaks split into two when additional plateaus appear due to Rashba SOI.

V. SUMMARY

We have studied quantum magnetotransport coefficients of k -cubic Rashba spin-orbit coupled two-dimensional fermionic systems. Our numerical analysis shows the appearance of beating patterns in the SdH oscillations. By drawing analogy with the Rashba spin-orbit coupled 2DEG at heterostructure, we proposed empirical forms of the oscillation frequencies of the spin-split fermions. It yields excellent matching of the locations of the nodes and number of oscillations between any two successive nodes obtained from the exact numerical calculations. On contrary to the complicated expression (see Eq. 6.39 in Ref. [13]) for determining spin-orbit coupling constant, we have obtained alternative and simple expressions (see Eq. (17) in this article) to determine it. The longitudinal resistivity peaks split into two unequal peaks at high magnetic field. We also found additional Hall plateaus in between any two integer quantum Hall plateaus. The appearance of additional Hall plateaus is due to the spin-orbit interaction. The width of this additional plateau increases with the spin-orbit coupling.

Appendix A: Energy Spectrum

Here we shall derive the energy spectrum and the corresponding eigenstates of the Hamiltonian H given by Eq. (1). With the choice of the Landau gauge $\mathbf{A} = (0, xB, 0)$, k_y is a good quantum number since $[H, p_y] = 0$. It allows us to write the wave function as $\psi(x, y) \sim e^{ik_y y} \Phi(x)$. Now the Hamiltonian H can be expressed as

$$H = \begin{pmatrix} a^\dagger a + \frac{1}{2} - \chi & \sqrt{8}\tilde{\alpha}a^{\dagger 3} \\ \sqrt{8}\tilde{\alpha}a^3 & a^\dagger a + \frac{1}{2} + \chi \end{pmatrix} \hbar\omega_c, \quad (\text{A1})$$

where $a^\dagger = -(il_c/\sqrt{2}\hbar)\Pi_-$ and $a = (il_c/\sqrt{2}\hbar)\Pi_+$ are the ladder operators such that $a^\dagger\phi_n = \sqrt{n+1}\phi_{n+1}$ and

$a\phi_n = \sqrt{n}\phi_{n-1}$, respectively. Here,

$$\phi_n(X) = \frac{1}{\sqrt{\sqrt{\pi}l_c 2^n n!}} H_n(X/l_c) e^{-X^2/2l_c^2}$$

are the harmonic oscillator states with $H_n(X)$ being the Hermite polynomial of order n , $X = x - x_c$.

As seen from Eq. (A1), one can take one of the following forms for the wave function $\Phi(X)$:

$$\Phi(X) = \begin{pmatrix} \phi_n(X) \\ D\phi_{n-3}(X) \end{pmatrix} \text{ or } \Phi(X) = \begin{pmatrix} D'\phi_n(X) \\ \phi_{n-3}(X) \end{pmatrix} \quad (\text{A2})$$

which is valid for $n \geq 3$.

Substituting Eq.(A2) in the time-independent Schroedinger equation $H\Phi(x) = E\Phi(x)$, we get

$$\begin{aligned} n + 1/2 - \chi + D\tilde{E}_{n\alpha} &= \varepsilon_n \\ \tilde{E}_{n\alpha} + D(n - 3 + 1/2 + \chi) &= D\varepsilon_n \end{aligned} \quad (\text{A3})$$

and

$$\begin{aligned} D'(n + 1/2 - \chi) + \tilde{E}_{n\alpha} &= \varepsilon_n D' \\ D'\tilde{E}_{n\alpha} + n - 3 + 1/2 + \chi &= \varepsilon_n, \end{aligned} \quad (\text{A4})$$

where $\tilde{E}_{n\alpha} = \sqrt{8n(n-1)(n-2)}\tilde{\alpha}$ and $\varepsilon_n = E_n/(\hbar\omega_c)$.

By solving either Eq.(A3) or Eq.(A4) we get the same energy spectrum

$$E_n^\lambda = \hbar\omega_c \left[n - 1 + \lambda \sqrt{\tilde{E}_{n\alpha}^2 + \tilde{E}_0^2} \right], \quad (\text{A5})$$

where $\lambda = \pm$ and $\tilde{E}_0 = 3/2 - \chi$.

Putting $\varepsilon_n^+ = n - 1 + \sqrt{\tilde{E}_{n\alpha}^2 + \tilde{E}_0^2}$ in Eq.(A3) and $\varepsilon_n^- = n - 1 - \sqrt{\tilde{E}_{n\alpha}^2 + \tilde{E}_0^2}$ in Eq.(A4), we get

$$D = D_n = \frac{\tilde{E}_{n\alpha}}{\tilde{E}_0 + \sqrt{\tilde{E}_0^2 + \tilde{E}_{n\alpha}^2}} \quad (\text{A6})$$

and $D' = -D = -D_n$. The normalization factor is $1/\sqrt{A_n}$ where $A_n = 1 + D_n^2$. Thus

$$\Phi_n^+(X) = \frac{1}{\sqrt{A_n}} \begin{pmatrix} \phi_n(X) \\ D_n\phi_{n-3}(X) \end{pmatrix} \quad (\text{A7})$$

and

$$\Phi_n^-(X) = \frac{1}{\sqrt{A_n}} \begin{pmatrix} -D_n\phi_n(X) \\ \phi_{n-3}(X) \end{pmatrix} \quad (\text{A8})$$

For $n < 3$, there are no spin split states, one can choose

$$\psi_{n,k_y}(x, y) = \frac{e^{ik_y y}}{\sqrt{L_y}} \phi_n(X) \begin{pmatrix} 1 \\ 0 \end{pmatrix}. \quad (\text{A9})$$

which will similarly give us

$$E_n = \left[n + \frac{1}{2} - \chi \right] \hbar\omega_c. \quad (\text{A10})$$

Appendix B: Form Factors

The square of the form factors $|F_{\xi, \xi'}|^2$ for $n \geq 3$ are given by

$$|F_{n, n'}^{++}(q)|^2 = \frac{1}{A_n A_{n'}} \frac{n!}{n!} u^{n-n'} e^{-u} \delta_{k'_y, k_y + q_y} \times \left[L_{n'}^{n-n'}(u) + D_n D_{n'} M_{n, n'} L_{n'-3}^{n-n'}(u) \right]^2 \quad (\text{B1})$$

and

$$|F_{n, n'}^{--}(q)|^2 = \frac{1}{A_n A_{n'}} \frac{n!}{n!} u^{n-n'} e^{-u} \delta_{k'_y, k_y + q_y} \times \left[D_n D_{n'} L_{n'}^{n-n'}(u) + M_{n, n'} L_{n'-3}^{n-n'}(u) \right]^2, \quad (\text{B2})$$

where $u = q^2 l_c^2 / 2$ and $M_{n, n'} = \sqrt{n(n-1)(n-2)/(n'(n'-1)(n'-2))}$.

For $n < 3$ we have the following form

$$|F_{nn}|^2 = e^{-u} L_n^2(u). \quad (\text{B3})$$

Appendix C: Matrix elements of velocity operator

Using Heisenberg equation of motion $v_i = (1/i\hbar)[x_i, H]$, we calculate the following components of the velocity operator

$$v_x = \frac{\Pi_x}{m^*} + \frac{3i\alpha}{2\hbar^3} (\sigma_+ \Pi_-^2 - \sigma_- \Pi_+^2) \quad (\text{C1})$$

and

$$v_y = \frac{\Pi_y}{m^*} + \frac{3\alpha}{2\hbar^3} (\sigma_+ \Pi_-^2 + \sigma_- \Pi_+^2). \quad (\text{C2})$$

The diagonal components of the velocity matrix elements are given by

$$\langle \zeta, + | v_x | \zeta', + \rangle = ia(B_{n-1} \delta_{n', n-1} - B_n \delta_{n', n+1}), \quad (\text{C3})$$

$$\langle \zeta, - | v_x | \zeta', - \rangle = ia(K_{n-1} \delta_{n', n-1} - K_n \delta_{n', n+1}), \quad (\text{C4})$$

$$\langle \zeta, + | v_y | \zeta', + \rangle = -a(B_n \delta_{n', n+1} + B_{n-1} \delta_{n', n-1}), \quad (\text{C5})$$

and

$$\langle \zeta, - | v_y | \zeta', - \rangle = -a(K_n \delta_{n', n+1} + K_{n-1} \delta_{n', n-1}), \quad (\text{C6})$$

where $a = \omega_c l_c \delta_{k'_y, k_y}$, $|\zeta\rangle = |n, k_y\rangle$, $B_n = (G_n + 6\tilde{\alpha} D_{n+1} \sqrt{n(n-1)}) / \sqrt{A_n A_{n+1}}$, $K_n = (F_n - 6\tilde{\alpha} D_n \sqrt{n(n-1)}) / \sqrt{A_n A_{n+1}}$ with $G_n = \sqrt{(n+1)/2} + D_n D_{n+1} \sqrt{(n-2)/2}$, and $F_n = D_n D_{n+1} \sqrt{(n+1)/2} + \sqrt{(n-2)/2}$.

The off-diagonal components of the velocity matrix elements are given by

$$\langle \zeta, + | v_x | \zeta', - \rangle = ia(K'_n \delta_{n', n+1} - B'_{n-1} \delta_{n', n-1}), \quad (\text{C7})$$

$$\langle \zeta, - | v_x | \zeta', + \rangle = ia(B'_n \delta_{n', n+1} - K'_{n-1} \delta_{n', n-1}), \quad (\text{C8})$$

$$\langle \zeta, + | v_y | \zeta', - \rangle = a(K'_n \delta_{n', n+1} + B'_{n-1} \delta_{n', n-1}), \quad (\text{C9})$$

$$\langle \zeta, - | v_y | \zeta', + \rangle = a(B'_n \delta_{n', n+1} + K'_{n-1} \delta_{n', n-1}), \quad (\text{C10})$$

where $B'_n = (G'_n + 6\tilde{\alpha} D_n D_{n+1} \sqrt{n(n-1)}) / \sqrt{A_n A_{n+1}}$, $K'_n = (F'_n - 6\tilde{\alpha} \sqrt{n(n-1)}) / \sqrt{A_n A_{n+1}}$ with $G'_n = D_n \sqrt{(n+1)/2} - D_{n+1} \sqrt{(n-2)/2}$ and $F'_n = D_{n+1} \sqrt{(n+1)/2} - D_n \sqrt{(n-2)/2}$.

¹ E. I. Rashba, Sov.Phys. Solid State **2**, 1109 (1960).

² Y. A. Bychkov and E. I. Rashba, J. Phys. C: Solid State Phys. **17**, 6039 (1984).

³ J. Nitta, T. Akazaki, H. Takayanagi, and T. Enoki, Phys. Rev. Lett. **78**, 1335 (1997).

⁴ T. Matsuyama, R. Kursten, C. Meibner, and U. Merkt, Phys. Rev. B **61**, 15588 (2000).

⁵ S. J. Papadakis, E. P. De Poortere, H. C. Manoharan, J. B. Yau, M. Shayegan, and S. A. Lyon, Phys. Rev. B **65**, 245312 (2002).

⁶ S. Datta and B. Das, Appl. Phys. Lett. **56**, 665 (1990).

⁷ S. Bandyopadhyay and M. Cahay, Introduction to Spin-

tronics (CRC press-2008).

⁸ I. Zutic, J. Fabian, and S. Das Sarma, Rev. Mod. Phys. **76**, 323 (2004).

⁹ J. Fabian, A. Matos-Abiague, C. Ertler, P. Stano, and I. Zutic, Acta Physica Slovaca **57**, 565(2007).

¹⁰ R. Winkler, Phys. Rev. B **62**, 4245 (2000).

¹¹ J. Schliemann and D. Loss, Phys. Rev. B **71**, 085308 (2005).

¹² B. A. Bernevig and S. C. Zhang, Phys. Rev. Lett. **95**, 016801 (2005).

¹³ R. Winkler, Spin-Orbit Coupling Effects in Two-Dimensional Electron and Hole Systems (Springer Verlag-

- 2003).
- ¹⁴ H. Nakamura, T. Koga, and T. Kimura, Phys. Rev. Lett. **108**, 206601 (2012).
 - ¹⁵ Z. Zhong, A. Toth, and K. Held, Phys. Rev. B **87**, 161102(R), (2013).
 - ¹⁶ R. Moriya et al., Phys. Rev. Lett. **113**, 086601 (2014).
 - ¹⁷ J. M. Luttinger and W. Kohn, Phys. Rev. **97**, 869 (1955).
 - ¹⁸ J. M. Luttinger, Phys. Rev. **102**, 1030 (1956).
 - ¹⁹ B. Grbic, R. Leturcq, T. Ihn, K. Ensslin, D. Reuter, and A. D. Wieck, Phys. Rev. B **77**, 125312 (2008).
 - ²⁰ Y. T. Chiu, M. Padmanabhan, T. Gokmen, J. Shabani, E. Tutuc, M. Shayegan, and R. Winkler, Phys. Rev. B **84**, 155459 (2011).
 - ²¹ T. M. Lu, Z. F. Li, D. C. Tsui, M. J. Manfra, L. N. Pfeiffer, and K. W. West, Appl. Phys. Lett. **92**, 012109 (2008).
 - ²² F. Nichele, A. N. Pal, R. Winkler, C. Gerl, W. Wegscheider, T. Ihn, and K. Ensslin, Phys. Rev. B **89**, 081306 (R) (2014).
 - ²³ R. Winkler, S. J. Papadakis, E. P. De Poortere, and M. Shayegan, Phys. Rev. Lett. **85**, 4574 (2000).
 - ²⁴ R. Winkler, Phys. Rev. B **71**, 113307 (2005).
 - ²⁵ M. G. Pala, M. Governale, J. König and U. Zulicke, and I. Iannaccone, Phys. Rev. B **69**, 045304 (2004).
 - ²⁶ S. Murakami, N. Nagaosa, and S. C. Zhang, Science **301**, 1348 (2003).
 - ²⁷ J. Wunderlich, B. Kaestner, J. Sinova, and T. Jungwirth, Phys. Rev. Lett. **94**, 047204 (2005).
 - ²⁸ M. W. Wu and J. Zhou, Phys. Rev. B **72**, 115333 (2005).
 - ²⁹ K. Nomura, J. Wunderlich, J. Sinova, B. Kaestner, A. H. MacDonald, and T. Jungwirth, Phys. Rev. B **72**, 245330 (2005).
 - ³⁰ W. Q. Chen, Z. Y. Weng, and D. N. Sheng, Phys. Rev. B **72**, 235315 (2005).
 - ³¹ P. Kleinert and V. V. Bryksin, Phys. Rev. B **76**, 073314 (2007).
 - ³² L. F. Mattheiss, Phys. Rev. B **6**, 4718 (1972).
 - ³³ R. Bistritzer, G. Khalsa, and A. H. MacDonald, Phys. Rev. B **83**, 115114 (2011).
 - ³⁴ Z. S. Popovic, S. Satpathy, and R. M. Martin, Phys. Rev. Lett. **101**, 256801 (2008).
 - ³⁵ A. F. Santander-Syro et al., Nature (London) **469**, 189 (2011).
 - ³⁶ T. Ma and Q. Liu, Appl. Phys. Lett. **89**, 112102 (2006).
 - ³⁷ M. Zarea and S. E. Ulloa, Phys. Rev. B **73**, 165306 (2006).
 - ³⁸ G. M. Eliashberg, Sov. Phys. JETP **14**(4), 866 (1962).
 - ³⁹ M. Charbonneau, K. M. van Vliet, and P. Vasilopoulos J. Math. Phys. **23**, 318 (1982).
 - ⁴⁰ P. Vasilopoulos and C. M. Van Vliet, J. Math. Phys. **25**, 1391 (1984).
 - ⁴¹ P. Vasilopoulos, Phys. Rev. B **32**, 771 (1985).
 - ⁴² F. M. Peeters and P. Vasilopoulos, Phys. Rev. B **46**, 4667 (1992).
 - ⁴³ X. F. Wang and P. Vasilopoulos, Phys. Rev. B **67**, 085313 (2003).
 - ⁴⁴ A. D. Caviglia, S. Gariglio, C. Cancellieri, B. Sacepe, A. Fete, N. Reyren, M. Gabay, A. F. Morpurgo, and J.M. Triscone, Phys. Rev. Lett. **105**, 236802 (2010).
 - ⁴⁵ M. M. Fogler and Shklovskii, Phys. Rev. B **52**, 17366 (1995).
 - ⁴⁶ Z. Q. Yuan, R. R. Du, M. J. Manfra, L. N. Pfeiffer, and K. W. West, Appl. Phys. Lett. **94**, 052103 (2009).
 - ⁴⁷ SK F. Islam and T. K. Ghosh, J. Phys.: Condens. Matter. **24**, 035302 (2012).